Acta Crystallographica Section A
Foundations of Crystallography
ISSN 0108-7673

Received 9 July 2004
Accepted 13 January 2005

A study of charge density in copper

J. Friis,[a]* B. Jiang,[b] K. Marthinsen[c] and R. Holmestad[a]

[a]Department of Physics, Norwegian University of Science and Technology (NTNU), N-7491 Trondheim, Norway, [b]Department of Physics and Astronomy, Arizona State University, Tempe, AZ 85287-1504, USA, and [c]Department of Materials Technology, Norwegian University of Science and Technology (NTNU), N-7491 Trondheim, Norway. Correspondence e-mail: jesper.friis@phys.ntnu.no

Quantitative convergent-beam electron diffraction (QCBED) experiments allow absolute scale measurements of low-order structure factors with very high accuracy. In this paper, eight low-order structure factors for copper measured by QCBED have been combined with the higher-order γ-ray structure factors in order to obtain a larger highly accurate experimental data set. The γ-ray values were relativistically corrected and rescaled. The new data set was then used for studying the charge distribution in copper. Charge deformation maps have been produced and both a maximum-entropy and a multipole analysis have been applied to the data. The result is compared to density functional theory calculations. An almost spherical charge depletion is found around the atomic sites showing typical metal bonding in copper.

1. Introduction

Recently, very accurate measurements of low-order structure factors in copper have been performed (Friis *et al.*, 2003). In this work, we have further enhanced the accuracy of the measurements. The new data set is then combined with the corrected (Petrillo *et al.*, 1998) γ-ray measurements of Schneider *et al.* (1981), and used for a more detailed study of the charge distribution in copper.

The deformation density, defined as the difference between the observed density and the procrystal density obtained from the independent-atom model (IAM), describes the redistribution of electronic charge due to bonding. Since this charge redistribution mainly occurs in the valence region with slow variations in the charge density, the bonding effect is mainly seen in the differences in the lowest-order structure factors. Since these differences are very small (around or less than 1%), very accurate measurements are required. Such an accuracy is difficult to obtain for the strong low-order reflections using ordinary X-ray or γ-ray diffraction owing to extinction and the contribution of anomalous scattering. Here we overcome this problem by measuring the lowest-order reflections with convergent-beam electron diffraction (CBED), which is very sensitive at small scattering angles.

Copper has for a long time been used as a test case for theoretical models of crystalline elements containing the complicated *d*-electron bands. It is non-magnetic and is relatively uncomplicated by relativistic effects because of its small mass. It is therefore not surprising that there have been many experimental measurements of the structure factors in copper.

By using γ-ray diffractometry, Schneider *et al.* (1981) could reduce the anomalous scattering and extinction effects in copper compared to earlier powder and single-crystal X-ray experiments (Batterman *et al.*, 1961; Jennings *et al.*, 1964; Hosoya & Yamagishi, 1966; Temkin *et al.*, 1972; Freud, 1973). However, the available scattering angles were at the same time reduced. Since it is difficult to obtain large perfect crystals of copper, required for traditional X-ray *Pendellösung* experiments, Takama & Sato (1982) measured a few low-order structure factors using a white-beam X-ray *Pendellösung* method. Although not as accurate as the ordinary *Pendellösung* method, this technique does not require such large single crystals. More recently, accurate structure factors have been measured by electron diffraction techniques. A big advantage of these methods is that they are performed in a transmission electron microscope (TEM), making it possible to select a perfect single-crystalline region for the experiment. However, the accuracy of these techniques is reduced for higher-order structure factors. Smart & Humphreys (1980) and Fox & Fisher (1988, cited in Tabbernor *et al.*, 1990) used the critical-voltage method, which is capable of measuring the ratio between structure factors as accurately as 0.1%. A limitation is that this method relies upon the accuracy of the reference used. The intersecting Kikuchi-line method, proposed by Gjønnes & Høier (1971), uses the sensitivity of the separation between high-order Kikuchi lines to certain structure factors. This method was combined with CBED by Matsuhata *et al.* (1984) for measuring the 111 and 020 reflections of copper. However, the most accurate experiments on copper so far are probably the quantitative CBED (QCBED) measurements by Saunders *et al.* (1999) and Friis *et al.* (2003). The strong multiple scattering of the electrons is here fully taken into account by using dynamical theory, which at the same time eliminates extinction and scaling problems. More detailed

overviews of the above experiments on copper can be found in Tabbernor *et al.* (1990), Mackenzie & Mathieson (1992) and Friis *et al.* (2003).

The γ-ray experiment by Schneider *et al.* (1981) is the most referred to structure-factor measurement for copper. The reasons for this probably are the good internal consistency of the data and that the data set is comparably large; 19 structure factors were measured up to $\sin\theta/\lambda = 1.6$ Å^{-1} at 50 K and room temperature (Schneider, 1976). However, compared to other experiments, these structure factors are somewhat low. The absolute scale and even the extinction correction of the γ-ray data has therefore been questioned, and several different corrections have been proposed. By applying an improved extinction correction scheme to the 220 structure factor, Mackenzie & Mathieson (1984) obtained a value closer to that of other experiments. On the other hand, Tabbernor *et al.* (1990) pointed out that good agreement can also be achieved by rescaling the data set to fit the 111 reflection of Fox & Fisher (1988). The idea that the discrepancy is due to problems with absolute scale, and not to the extinction correction, is also approved by Schneider (Tabbernor *et al.*, 1990). In a new analysis of Schneider *et al.*'s (1981) data, Petrillo *et al.* (1998) chose a slightly smaller Debye–Waller factor for Cu at 50 K. More importantly, Petrillo *et al.* (1998) applied a kinematic correction (in the order of the experimental errors), whose importance was first realized by Dewey *et al.* (1994). This correction is due to the relativistic energies of the γ rays and can be interpreted as a relativistic change of the electron mass. Finally, a scaling factor of 1.0042 (62) was introduced in order to fit the relativistic Hartree–Fock free-atom structure factors (Doyle & Turner, 1968) for scattering angles $\sin\theta/\lambda > 0.5$ Å^{-1}.

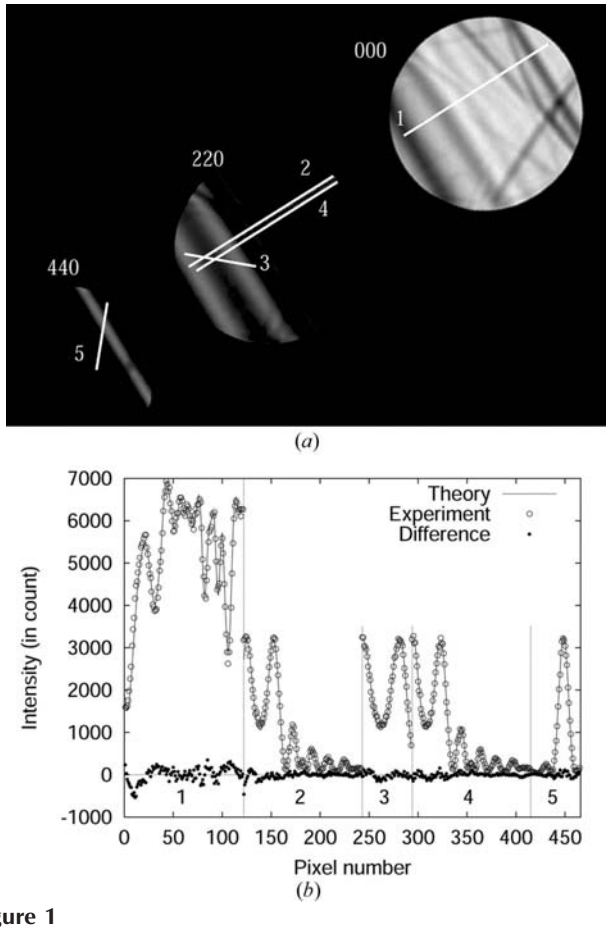

Figure 1
(*a*) CBED pattern of the 220 systematic row in copper. The selected rocking curves are shown with white lines. (*b*) Best fit from Bloch-wave refinement of the selected rocking curves. The open circles are measured intensities while the solid line is calculated intensities. The discrepancy for each pixel between theory and experiment is also shown with dots.

The aim of the current paper is to enhance the experimental data (Friis *et al.*, 2003) and to compare different ways to obtain charge deformation maps. In particular, it includes the use of the maximum-entropy method as a method to analyse QCBED results.

We have in this paper slightly improved the already published QCBED measurements (Friis *et al.*, 2003) of low-order structure factors in copper by including a few more measurements and by re-evaluating the Debye–Waller factor of copper at experimental temperature (§2). In §3, these structure factors have then been combined with higher-order γ-ray diffractometry measurements by Schneider *et al.* (1981). Before combination, the above-mentioned relativistic correction was applied and new Debye–Waller and scaling factors were derived for the γ-ray data. We have also applied a small correction due to the difference in lattice parameter between the CBED (close to 112 K) and γ-ray (50 K) experiments.

Using the combined data set, new charge deformation maps have been calculated using direct Fourier synthesis (§4), the maximum-entropy method (MEM) (§5) and the multipole model presented in Jiang *et al.* (2004) (recapitulated in §6). Finally, in §7, the new data set is compared with other experiments and theoretical calculations and the different deformation density maps are compared and discussed.

2. QCBED measurements of structure factors

In the CBED technique, the electron probe in the TEM is focused down to the size of a few nanometres. This makes it easy to study perfectly crystalline regions of the sample. Since the CBED patterns show the rocking curve of every diffracted beam simultaneously, they are well suited for quantitative work (Spence & Zuo, 1992; Zuo, 2004). Because electrons interact strongly with the crystal potential and are multiply scattered when they pass through the sample, a full dynamic theory is required when analysing the CBED patterns. Extinction, which is a problem in X-ray diffraction for the strong low-order reflections in small unit-cell crystals, is therefore fully accounted for in QCBED. The QCBED method is based on a pixel-to-pixel comparison between the experiment and a Bloch-wave simulation, where some of the low-order Fourier coefficients of the crystal potential $V_{\mathbf{h}}$ are treated as refinable parameters (Zuo, 1998). A typical CBED pattern is shown in Fig. 1(*a*) for the 220 systematic row with some line scans, sensitive to the refined parameters, marked on it. Fig. 1(*b*) shows the best fit along the chosen line scans obtained with the Bloch-wave simulation.

Table 1
Selected theoretical and experimental static lattice scattering factors for Cu.

The data set is complete up to 440 but after that 39 structure factors are missing up to 880. The column labelled 'combined' is the same as this experiment, but with the missing values replaced by the corrected γ-ray data. The agreement factors $R_{\rm this\,exp}$ and $R_{\rm combined}$ are given by $R = \left(\sum ||F| - |F^{\rm ref}||\right)/\sum |F^{\rm ref}|$ and show the agreement between this experiment and the combined data, respectively.

					Schneider *et al.* (1981)							
h k l	$\sin\theta/\lambda$ (Å^{-1})	IAM†	Bagayoko *et al.* (1980)	DFT‡	Original values	Δ§	Corrected values ¶	Saunders *et al.* (1999)	This experiment (2003)	Combined	MEM	Multipole analysis
1 1 1	0.24	22.05	21.68	21.70	21.51 (5)	−0.06	21.73 (5)	21.78 (2)	21.69 (3)	21.69 (3)	21.84	21.71
2 0 0	0.28	20.69	20.35	20.38	20.22 (4)	−0.07	20.43 (4)	20.44 (2)	20.44 (2)	20.44 (2)	20.47	20.41
2 2 0	0.39	16.74	16.62	16.67	16.45(5)	−0.08	16.63 (5)	16.7 (1)	16.68 (2)	16.68 (2)	16.70	16.67
3 1 1	0.46	14.74	14.70	14.75	14.54 (4)	−0.08	14.70 (4)	14.8 (1)	14.73 (1)	14.73 (1)	14.72	14.74
2 2 2	0.48	14.19	14.17	14.21	14.07 (5)	−0.08	14.22 (5)		14.24 (7)	14.24 (7)	14.20	14.21
4 0 0	0.56	12.42	12.42	12.48	12.29 (6)	-0.08	12.42 (6)		12.45 (9)	12.45 (9)	12.43	12.46
3 3 1	0.60	11.42	11.41	11.47	11.30††	−0.09	11.42 (9)			11.42 (9)	11.42	11.46
4 2 0	0.62	11.13	11.13	11.19	11.02 (6)	−0.09	11.1 (1)		11.18 (9)	11.18 (9)	11.14	11.18
4 2 2	0.68	10.16	10.16	10.21	10.08 (6)	−0.09	10.2 (1)			10.2 (1)	10.16	10.20
3 3 3	0.72	9.58	9.58	9.63	9.49 (6)	−0.09	9.59 (9)			9.59 (9)	9.58	9.62
5 1 1	0.72	9.58	9.58	9.64	9.53 (6)	−0.09	9.63 (9)			9.63 (9)	9.58	9.62
4 4 0	0.78	8.82		8.86	8.84 (8)	−0.09	8.9 (1)		8.85 (2)	8.85 (2)	8.84	8.86
6 0 0	0.83	8.35		8.40	8.37 (9)	−0.09	8.5 (1)			8.5 (1)	8.36	8.39
4 4 4	0.96	7.38		7.40	7.33 (9)	−0.09	7.4 (1)			7.4 (1)	7.38	7.41
8 0 0	1.11	6.64		6.66	6.8 (1)	−0.09	6.8 (2)			6.8 (2)	6.65	6.65
6 6 0	1.18	6.37		6.37	6.4 (1)	−0.09	6.4 (2)			6.4 (2)	6.38	6.37
5 5 5	1.20	6.28		6.27	6.3 (1)	−0.09	6.3 (2)			6.3 (2)	6.29	6.28
10 0 0	1.39	5.66		5.65	5.6 (2)	−0.09	5.6 (2)			5.6 (2)	5.65	5.65
6 6 6	1.44	5.49		5.49	5.5 (2)	−0.09	5.5 (2)			5.5 (2)	5.49	5.49
8 8 0	1.57	5.09		5.09	5.1 (2)	0.09	5.1(2)			5.1 (2)	5.09	5.09
$R_{\rm this\,exp}$ (%)		0.69	0.31	0.15	1.09		0.24	0.24	–		0.27	0.10
$R_{\rm combined}$(%)		0.64	0.30	0.30	0.96		0.14	0.24		–	0.38	0.28

† Calculated from Doyle & Turner (1968). ‡ Calculated with the *WIEN2k* program of Blaha *et al.* (2001). § Relativistic correction of the γ-ray structure factors from Petrillo *et al.* (1998). ¶ Estimated standard uncertainties are from Petrillo *et al.* (1998). †† Estimated by interpolation.

For bonding studies, the interesting quantity is the electron density, of which Fourier components are the X-ray structure factors $F_{\mathbf{h}}$. These are directly related to $V_{\mathbf{h}}$ through the reciprocal-space version of Poisson's equation (also known as the Mott–Bethe formula). The operation of this equation provides increased sensitivity to the low-order structure factors (Spence & Zuo, 1992).

The structure factors reported in Table 1 under 'this experiment' are based on the experiments published in Friis *et al.* (2003), including some new refinements and with a few problematic (not perfectly focused, contaminated or low-exposed) CBED patterns replaced with new experiments. The new experiments and refinements were performed in the same way as earlier described in Friis *et al.* (2003) and the same lattice parameter $a = 3.60540\,(3)$ Å was used. These additions have not led to any significant changes in the structure-factor values, but the errors are somewhat decreased due to better statistics. More notable is that the value of the 420 structure factor has been added to the data set and a new value of the Debye–Waller factor has been used. In Friis *et al.* (2003), the Debye–Waller factor was estimated solely from the extra carefully measured 440 reflection. In this work, however, Wilson plot fitting is used in order to include all the measured reflections in the determination of the Debye–Waller factor. The basic idea is to estimate the temperature factor $\exp(-Bs^2)$ by least-squares fitting of the measured scattering factor $f^{\rm exp}(s)$ to $\exp(-Bs^2)f^0(s)$, where $f^0(s)$ is the theoretical static lattice scattering factor, B is the Debye–Waller factor and $s = \sin\theta/\lambda$ is the scattering angle. Normally, high-order reflections are used for Wilson plot fitting since they are more sensitive to the temperature factor and not affected by bonding. However, with QCBED, only low-order structure factors are measured, so the bonding effects must be considered when calculating the static lattice scattering factors.

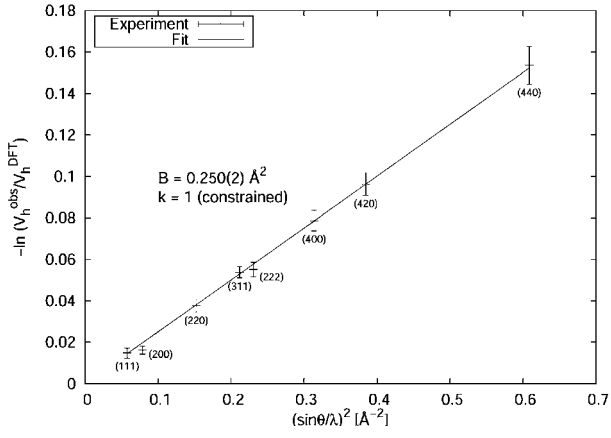

Figure 2
Wilson plot of the QCBED data at 112 K with DFT as static lattice reference. B is the Debye–Waller factor and k the scale factor (we assume QCBED to be on an absolute scale).

Hence, we have used DFT instead of the more commonly used scattering factors of Doyle & Turner (1968). Furthermore, since QCBED provides structure factors on an absolute scale, the scaling factor k is constrained to 1. This results in $B = 0.250\,(2)$ Å^2 at 112 K (Fig. 2), which agrees well with our previous value $B = 0.248$ Å^2.

Finally, a small correction, accounting for the difference in scattering angle between experimental temperature (112 K) and static lattice, has been applied to the measured structure factors. This can be approximated by multiplying the structure factors with a ratio $f(s^{0\mathrm{K}})/f(s^{112\mathrm{K}})$, where $f(s)$ are interpolated scattering factors (Doyle & Turner, 1968) depending on the scattering angle s^T, given by the lattice parameter at temperature T. Bonding effects are not important to consider here, since this correction is small and the ratio $f(s^{0\mathrm{K}})/f(s^{112\mathrm{K}})$ will tend to cancel the introduced errors.

3. Combination with γ-ray data

In order to reduce truncation errors due to the limited set of measured structure factors when studying the charge density, the QCBED data have been combined with the γ-ray measurements by Schneider *et al.* (1981) after subtraction of the small relativistic correction Δ calculated by Petrillo *et al.* (1998). In Fig. 3, the Debye–Waller factor and scale factor[1] are determined at 50 K from both the corrected and uncorrected structure factors. Again, DFT has been used as the static lattice reference allowing us to use the whole data set. It is seen that the kinematic correction gives rise to small but significant changes in the Debye–Waller factor and scale-factor values. It should also be noted that the Debye–Waller factor $B = 0.153\,(2)$ Å^2 obtained with the kinematic correction is identical to the value calculated by Svensson *et al.* (1969) at 50 K. The relativistically corrected structure factors listed in Table 1 are obtained by subtracting Δ from Schneider *et al.*'s (1981) original values and using $B = 0.153$ Å^2 and $k = 1.008$ instead of $B = 0.167$ Å^2 and $k = 1$ as used by Schneider *et al.* (1981). We have also applied the same increase in the standard uncertainties to these 'corrected' structure factors as used by Petrillo *et al.* (1998). In the column labelled 'combined', we have replaced the corrected structure factors by our QCBED measurements in those cases where they are available.

4. Charge deformation density of copper

The kinematic non-forbidden structure factors for Cu take the form

$$F(s) = 4f(s)\exp(-Bs^2), \qquad (1)$$

where $f(s)$ is the atomic scattering factor (or form factor). For the IAM, several good parameterizations of the scattering factors exist (Su & Coppens, 1997; Peng, 1998; Macchi & Coppens, 2001). The most famous and widely used are probably the relativistic Hartree–Fock scattering factors of Doyle & Turner (1968), which are used for the IAM in this paper. A commonly used quantity for recognition of bonding features is the experimental deformation density,

$$\Delta\rho(\mathbf{r}) = \frac{1}{V}\sum_{\mathbf{h}}(F_{\mathbf{h}}^{\mathrm{obs}} - F_{\mathbf{h}}^{\mathrm{IAM}})\exp(-2\pi i\mathbf{r}\cdot\mathbf{h}), \qquad (2)$$

defined as the difference between the crystal and the IAM densities. V is the unit-cell volume. The deformation density shows charge accumulation in bonding regions, but quantitative considerations cannot be drawn too far, since the deformation density depends on the definition of the reference density and is thermally averaged. Another practical limitation of deformation densities calculated from a set of measured structure factors is the errors due to series truncation. As shown in Fig. 4, these errors are mainly concentrated in high-symmetry regions. For copper, it is common to plot the charge density in the (110) plane since this plane contains both nearest, second-nearest and third-nearest neighbours. Fig. 5 shows the deformation density calculated from the 12 lowest-order structure factors in the combined data set. Since the data are only complete up to 440 ($\sin\theta/\lambda \leq 0.79$ Å^{-1}), higher orders are not included. The standard uncertainties of the deformation density, shown in Fig. 4, were calculated according to the formalism of Rees (1976) and Rees & Mitschler (1976). In accordance to this formalism, the truncation errors will accumulate close to high-symmetry sites, since these regions contain many symmetry-equivalent positions. The effect of the uncertainties in the scaling and Debye–Waller factors on the deformation density are negligible compared to the uncertainties shown in Fig. 4.

The deformation density in Fig. 5 seems to show, as expected from metallic bonded crystals, charge depletion at the atomic sites and a build up of charge in the interstitial regions. A maximum of 0.19 e Å^{-3} is seen at the interstitial octahedral sites. However, this maximum is not significant due to the large standard uncertainties, $\sigma(\Delta\rho) = 0.26$ e Å^{-3} at the octahedral sites.

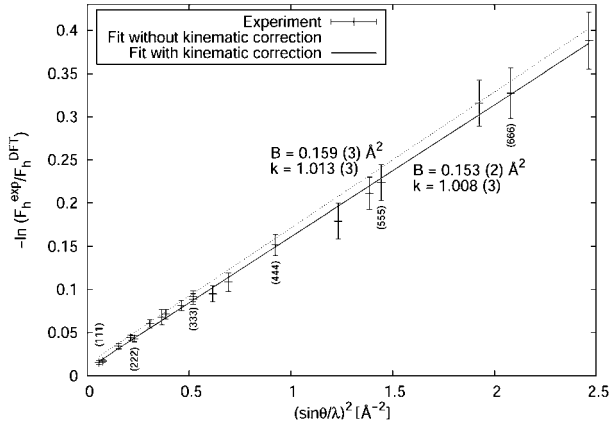

Figure 3
Wilson plot of γ-ray data at 50 K with DFT as static lattice reference. The Debye–Waller factor B and scaling factor k are shown for the best fit with (solid line) and without (dotted line) the kinematic Δ correction.

[1] The scale factor k is defined by $k|F^{\mathrm{exp}}| = \exp(-Bs^2)|F^0|$, where F^0 are static lattice structure factors.

In the following two sections, more sophisticated methods are used in order to deal with the truncation and other errors due to the incompleteness of the data.

5. Maximum-entropy fitting of direct-space charge density

The maximum-entropy method (MEM) is a method based on information theory to enhance information from limited or poor data. Applications in crystallography have been reviewed by Gilmore (1996). It has often been used to calculate the charge-density distribution from a limited set of structure factors (Collins, 1982; Sakata & Sato, 1990; Papoular *et al.*, 1996). The basic idea is to find the charge distribution that maximizes the entropy, under the constraint that structure factors calculated from this distribution must match the measured structure factors.

But, as pointed out by Jauch & Palmer (1993) and Jauch (1994), the traditional maximum-entropy algorithm is limited when fine details, such as bonding deformation, are to be studied, and the charge density to be reconstructed has a large dynamic range. However, if one uses the deformation density $\Delta\rho(\mathbf{r})$ as the key quantity when maximizing the entropy, the dynamic range is substantially reduced and the small bonding features become more pronounced. Since MEM relates the charge density directly to probabilities, the use of the deformation density, which takes both positive and negative values, requires a two-channel method. This method has successfully been used for magnetization densities (Papoular & Gillon, 1990), in neutron diffraction involving scattering lengths of opposite signs (Sakata *et al.*, 1993) and deformation densities (Papoular *et al.*, 1996).

In the two-channel method, the deformation density is split into two quantities, a positive $\rho^+(\mathbf{r})$ and a negative $\rho^-(\mathbf{r})$ part, such that $\Delta\rho(\mathbf{r}) = \rho(\mathbf{r}) - \rho^{\rm IAM}(\mathbf{r}) = \rho^+(\mathbf{r}) - \rho^-(\mathbf{r})$. The unit cell is divided into M pixels, each of size V/M centred at $\mathbf{r}_j$ and with densities $\rho_j^+ = \rho^+(\mathbf{r}_j)$ and $\rho_j^- = \rho^-(\mathbf{r}_j)$. The entropy functional to be maximized is given by

$$S[\Delta\rho] = -\sum_{j=1}^{M} [p_j^+ \ln p_j^+ + p_j^- \ln p_j^-], \qquad (3)$$

where $p_j^\pm = \rho_j^\pm / Q^\pm$, with $Q^\pm = \sum_{j=1}^M \rho_j^\pm$, are the corresponding probabilities for the positive and negative parts of the deformation density associated with pixel j. The maximization of $S[\Delta\rho]$ is performed under the constraint that the difference between the structure factors calculated from the MEM charge density and the IAM structure factors,

$$\Delta F_{\mathbf{h}}^{\rm calc} = \frac{V}{M} \sum_{j=1}^{M} (Q^+ p_j^+ - Q^- p_j^-) \exp(2\pi i \mathbf{h}\cdot\mathbf{r}), \qquad (4)$$

agrees with the difference between the N observed structure factors and IAM structure factors $\Delta F_{\mathbf{h}}^{\rm obs}$ within the standard uncertainty $\sigma_{\mathbf{h}}$. This condition is expressed as

$$\chi^2 = \frac{1}{N} \sum_{\mathbf{h}} \left(|\Delta F_{\mathbf{h}}^{\rm obs} - \Delta F_{\mathbf{h}}^{\rm calc}|^2 / \sigma_{\mathbf{h}}^2 \right) \lesssim 1. \qquad (5)$$

The problem is solved by maximizing the Lagrange functional $L[\rho] = S[\Delta\rho] - \lambda\chi^2$, where λ is the Lagrange multiplier. At convergence, $\nabla_\rho L = 0$, resulting in the normalized densities

$$p_j^\pm = m_j^\pm \exp\left(\mp\lambda \frac{\partial\chi^2}{\partial p^\pm} \right), \qquad (6)$$

where $m_j^\pm$ are prior density distributions. The deformation density is obtained by solving equations (4), (5) and (6) iteratively for both $p^\pm$ and λ, starting from a flat deformation density and $\lambda \gtrsim 0$.

It has been argued that a problem with two-channel MEM applied to the deformation density is that Q^+ and Q^- are unknown. However, since the total amount of charge is conserved in the formation of the deformation density, we must have $Q^+ = Q^- = Q$. It is then easy to show that, by introducing a scaled Lagrange multiplier $\Lambda = \lambda Q$, one can move all dependence of Q into this Lagrange multiplier. Hence, the value chosen for Q does not matter, since the Lagrange multiplier is already an unknown parameter that has to be given a suitable value in order to achieve convergence.

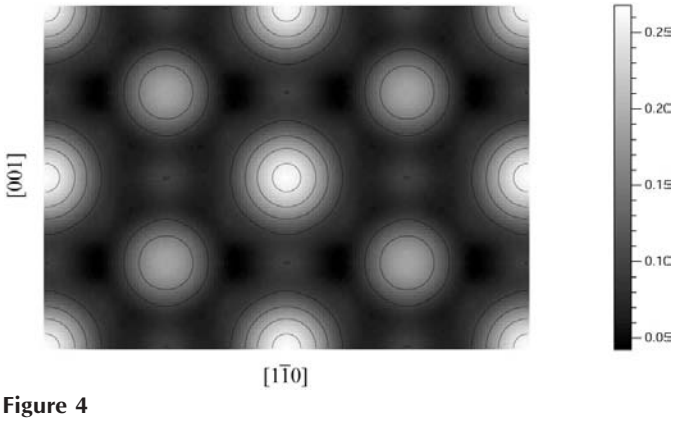

Figure 4
Standard uncertainty in the deformation density calculated from the combined data set, $\sin\theta/\lambda \leq 0.79$ Å^{-1}. The contour lines range from 0.1 to 0.25 e Å^{-3} with intervals of 0.05 e Å^{-3}.

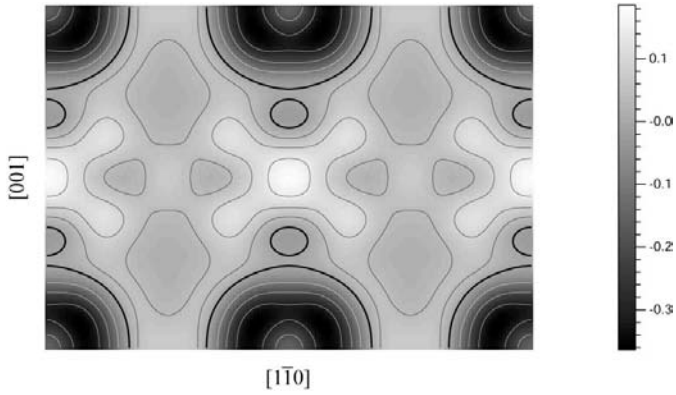

Figure 5
Electron deformation density calculated from the combined data set for $\sin\theta/\lambda \leq 0.79$ Å^{-1}. Negative contours (white) are at intervals of 0.1 e Å^{-3} and positive contours (black) are at intervals of 0.05 e Å^{-3}. The zero contour is shown as a thick line.

The *MEND* program (Sakata & Takata, 1994), modified by Burger (1998), was used to solve the problem. The unit cell was divided into $128 \times 128 \times 128$ pixels. In order to check that the algorithm only depends on the product of λ and Q, several different starting points with uniform prior deformation densities, $\Delta\rho^{+}_{0,j} = \Delta\rho^{-}_{0,j} = 0.05, 0.1, 1.0, 2.5$ e Å^{-3}, were tried. In all cases, the same convergence was achieved with λ_0 around $(5 \times 10^{-4}\,\text{e Å}^{-3})/\Delta\rho_{0,j}$. The same results were also obtained with smaller grids of $32 \times 32 \times 32$ and $64 \times 64 \times 64$ pixels.

The deformation density for $\Delta\rho^{+}_{0,j} = \Delta\rho^{-}_{0,j} = 0.05$ e Å^{-3} and $\lambda_0 = 0.01$ is shown in Fig. 6. This map is quite similar to the one obtained from direct Fourier synthesis. It shows an average interstitial charge surplus of 0.05 e Å^{-3} and a less pronounced peak at the interstitial octahedral sites.

Instead, small maxima are seen at the midpoint of the nearest-neighbour bond and at the tetrahedral sites.

6. Multipole analysis

In multipole analysis, the atomic charge density is expanded in terms of a series of multipolar functions centred at the nucleus. The multipole populations and radial expansion parameters are determined from least-squares fitting to the measured structure factors. This method has the advantage that it provides an analytical expression for the charge density, allowing for easy calculation of physical properties based on the charge distribution. Another interesting feature is that the multipole populations can be related to orbital occupancies.

In the valence-density formalism of Hansen & Coppens (1978), the atomic electron density

$$\rho_{\text{atom}}(\mathbf{r}) = P_{\text{c}}\rho_{\text{core}}(r) + P_{\text{v}}\kappa^3\rho_{\text{valence}}(\kappa r) + \sum_{l=0}^{l_{\max}} \kappa_l'^3 R_l(\kappa_l' r) \sum_{m=0}^{l} P_{lm\pm}\, d_{lm\pm}(\theta, \phi) \qquad (7)$$

is described by three parts: a spherical core part populated with P_c electrons, a spherical valence part which is allowed to expand ($\kappa < 1$) or contract ($\kappa > 1$) with population P_v and a series of multipolar functions accounting for an aspherically redistribution of the electron density, each populated with $P_{lm\pm}$ electrons. The multipolar functions are characterized by the radial functions $R_l(\kappa_l' r)$ and the density functions $d_{lm\pm}(\theta, \phi)$, which are density-normalized real spherical harmonics (Coppens, 1997, ch. 3). Because of the strong symmetry imposed by the cubic atom site symmetry of copper, all terms in the multipole expansion up to $l_{\max} = 3$, except for the monopole, will vanish (Kurki-Suonio, 1977). For the hexadecapoles ($l = 4$), only one independent cubic population parameter P_{hex} will remain.

In Jiang *et al.* (2004), a multipole analysis for the combined data set was performed. Assuming that the 3*d* radial wavefunction has a diffuse tail that does not contribute significantly to the measured reflections, a model that reproduces very well the observed structure factors could be obtained. This deformation of the 3*d* orbital was simulated by writing the 3*d* orbital as $3d_{\text{deformed}} = 3d^{10-n}4s^n$ with $n = 1.34$, where 3*d* and 4*s* here refers to Clementi & Roetti's (1974) Slater-type radial functions.

Applied to the new data set, this model results in a negligible aspherical contribution to the charge density in copper [$P_{\text{hex}} = -0.0000\,(2)$], which is also seen from the spherical charge depletion around the atomic sites in the model deformation-density map (Fig. 7) obtained by evaluating density functions in direct space. The fact that the spherical model seems to give a very good description of copper also validates the special construction of the $3d_{\text{deformed}}$ radial function.

7. Discussion and conclusions

For comparison, several sets of low-order scattering factors for copper are listed in Table 1. The theoretical values are the IAM scattering factors by Doyle & Turner (1968), the self-consistent band-structure calculation by Bagayoko *et al.* (1980) and a full-potential DFT calculation using the generalized gradient approximation (GGA) performed with *WIEN2k* (Blaha *et al.*, 2001). Experimental values are the γ-ray diffractometry measurements by Schneider *et al.* (1981), the QCBED experiments by Saunders *et al.* (1999) and the

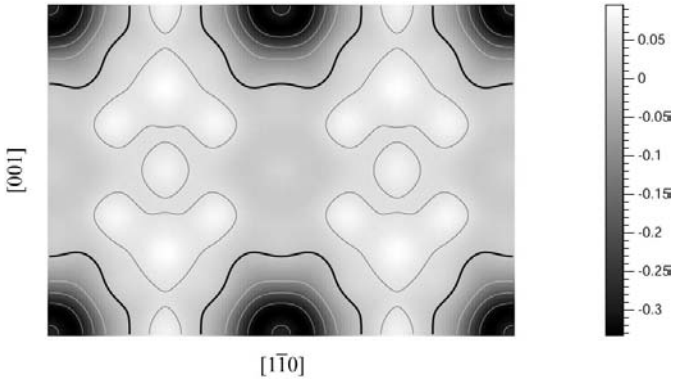

Figure 6
The deformation density from a two-channel MEM simulation. Negative contours (white) are at intervals of 0.1 e Å^{-3} and positive contours (black) are at intervals of 0.05 e Å^{-3}. The zero contour is shown as a thick line.

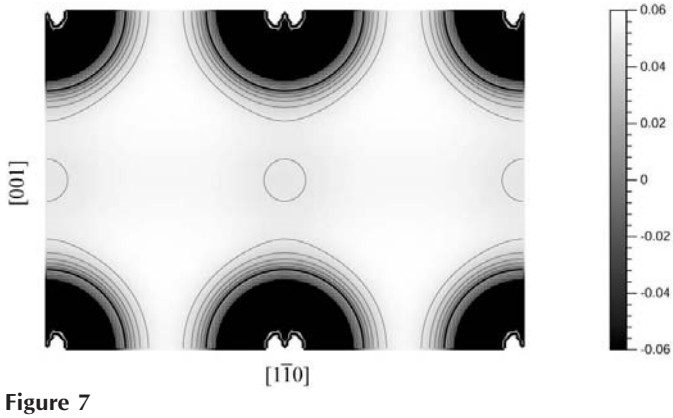

Figure 7
Model deformation density of the (110) plane from multipole analysis. The deformation density in the interstitial region is 0.05 e Å^{-3}. Contour intervals are 0.01 e Å^{-3}. The zero contour is shown as a thick line.

QCBED experiments presented in the present paper. The last two rows show the scattering factors obtained by applying the MEM and multipolar analysis to the combined data set. The difference between the scattering factors and the IAM values are plotted in Fig. 8 as well as the corresponding differences for the DFT, MEM, observed and multipole scattering factors.

As seen from Table 1, there is an inconsistency between the two QCBED measurements of the 111 structure factor. We do not have a satisfactory explanation for this, but it might be related to the fact that the small scattering angle of the 111 reflection leads to overlapping discs. In our systematic row approach, it is still easy to draw long line scans above or below the overlapping regions. However, in the zone-axis approach by Saunders, this may lead to problems.

The *R* factors in Table 1 show that correcting the γ-ray data leads to large improvements in the agreement between the γ-ray measurements and our experiment.

Compared to the old calculation by Bagayoko *et al.* (1980), the DFT calculations show a significant improvement in the *R* factor for our experiment. However, the agreement for the DFT calculations are worse when the higher-order corrected γ-ray data are also taken into account. Since the GGA method is usually more accurate for higher orders, this might imply that there are still some problems with the γ-ray data, despite the corrections.

In Jiang *et al.* (2004), it is seen from the DFT calculations that the scattering from the valence 3*d* and 4*s* orbitals is very small at $\sin\theta/\lambda = 0.8$ Å^{-1} and almost vanish for scattering angles larger than 1 Å^{-1}. One would therefore expect the true scattering factors to be very close to the IAM values for $\sin\theta/\lambda > 1.0$ Å^{-1}, which also is the case in Fig. 8.

It is clear from Fig. 8 that the multipole model fits the observed scattering factors very well.

However, an even better agreement is seen between DFT and the multipole model, which justifies our construction of the 3*d* multipolar orbital.

The model deformation density calculated by DFT is shown in Fig. 9. It is very similar to the multipolar model deformation density in Fig. 7. Both these maps show a spherical charge depletion at the atomic sites, typical for metallic bonding, but also a small charge surplus between the nearest neighbours.

The maximum-entropy method tends to move the structure factors toward the IAM values (Fig. 8), which are the structure factors maximizing the entropy for the two-channel method used in this work. This does not seem to provide much physical insight, but a smoother (and more realistic) charge density is obtained compared to direct Fourier synthesis. However, the MEM can be seen as a statistical method to potentially reduce the problems with incomplete data sets and truncation errors in deformation-density maps obtained by Fourier synthesis. And indeed, the MEM deformation-density map (Fig. 6) shows features similar to those from DFT (Fig. 9), but the radius of the spherical charge depletion around the nucleus is too small and the deformation density still shows some unphysical ripples.

In summary, DFT and the multipole model seem to provide a very good description of copper, which shows typical metallic bonding.

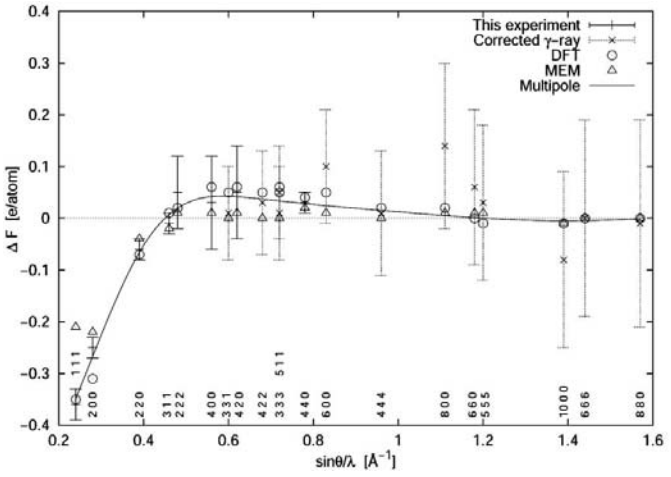

Figure 8
The difference between static lattice scattering factors and Doyle & Turner (1968) independent-atom values *versus* scattering angle. Units in e atom^{-1}. The solid line is for the multipole analysis.

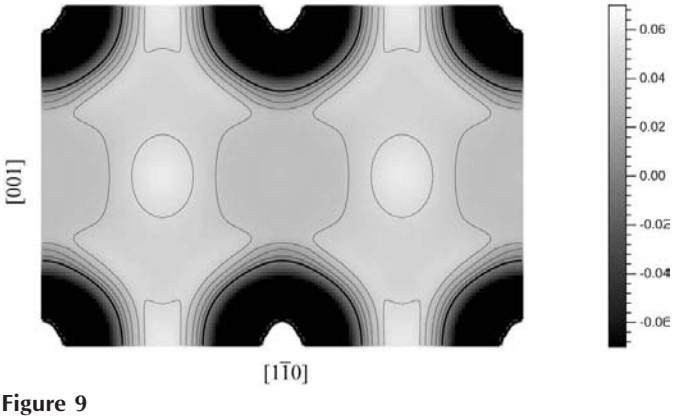

Figure 9
Model deformation density of the (110) plane calculated from density functional theory. Contour intervals are 0.01 e Å^{-3}. The zero contour is shown as a thick line.

We thank Professor J. C. H. Spence (Arizona State University) and Professor J. M. Zuo (University of Illinois) for helpful discussions. Funding from the Research Council of Norway (NFR), project 135270/410, is gratefully acknowledged. B. Jiang is funded by DOE DE-FG03-02ER45596.

References

Bagayoko, D., Laurent, D. G., Singhal, S. P. & Callaway, J. (1980). *Phys. Lett. A*, **76**, 187–190.

Batterman, B. W., Chipman, D. R. & Marco, J. J. D. (1961). *Phys. Rev.* **76**, 68–74.

Blaha, P., Schwarz, K., Madsen, G., Kvasnicka, D. & Luitz, J. (2001). *WIEN2k, an Augmented Plane Wave Plus Local Orbitals Program for Calculating Crystal Properties.* Vienna University of Technology, Austria.

Burger, K. (1998). *Enchanced Versions of the Maximum Entropy Program MEED for X-ray and Neutron Diffraction.* Institut für Kristallographie, Universität Tübingen, Germany.

Clementi, E. & Roetti, C. (1974). *At. Data Nucl. Data Tables*, **14**, 177–478.
Collins, D. M. (1982). *Nature (London)*, **298**, 49–51.
Coppens, P. (1997). *X-ray Charge Densities and Chemical Bonding.* Oxford University Press.
Dewey, M. S., Kessler, E. G., Greene, G. L., Deslattes, R. D., Sacchetti, F., Petrillo, C., Freund, A., Börner, H. G., Robinson, S. & Schillebeecks, P. (1994). *Phys. Rev. B*, **50**, 2800–2808.
Doyle, P. A. & Turner, P. S. (1968). *Acta Cryst.* A**24**, 390–397.
Fox, A. G. & Fisher, R. M. (1988). Unpublished.
Freud, A. (1973). PhD thesis, Technische Universität München, Germany.
Friis, J., Jiang, B., Spence, J. C. H. & Holmestad, R. (2003). *Microsc. Microanal.* **9**, 379–389.
Gilmore, C. (1996). *Acta Cryst.* A**52**, 561–589.
Gjønnes, J. & Høier, R. (1971). *Acta Cryst.* A**27**, 313–316.
Hansen, N. K. & Coppens, P. (1978). *Acta Cryst.* A**34**, 909–921.
Hosoya, S. & Yamagishi, T. (1966). *J. Phys. Soc. Jpn.* **21**, 2638–2644.
Jauch, W. (1994). *Acta Cryst.* A**50**, 650–652.
Jauch, W. & Palmer, A. (1993). *Acta Cryst.* A**49**, 590–591.
Jennings, L. D., Chipman, D. R. & Marco, J. J. D. (1964). *Phys. Rev.* **135**, 1612–1615.
Jiang, B., Friis, J., Holmestad, R., Zuo, J., O'Keeffe, M. & Spence, J. C. H. (2004). *Phys. Rev. B*, **69**, 245110.
Kurki-Suonio, K. (1977). *Isr. J. Chem.* **16**, 115–123.
Macchi, P. & Coppens, P. (2001). *Acta Cryst.* A**57**, 656–662.
Mackenzie, J. K. & Mathieson, A. (1984). *Aust. J. Phys.* **37**, 651–656.
Mackenzie, J. K. & Mathieson, A. (1992). *Acta Cryst.*, A**48**, 231–236.
Matsuhata, H., Tomokiyo, Y., Watanabe, H. & Eguchi, T. (1984). *Acta Cryst.* B**40**, 544–549.
Papoular, R. J. & Gillon, B. (1990). *Europhys. Lett.* **13**, 429–434.
Papoular, R. J., Vekhter, Y. & Coppens, P. (1996). *Acta Cryst.* A**52**, 397–407.
Peng, L. M. (1998). *Acta Cryst.* A**54**, 481–485.
Petrillo, C., Sacchetti, F. & Mazzone, G. (1998). *Acta Cryst.* A**54**, 468–480.
Rees, B. (1976). *Acta Cryst.* A**32**, 483–488.
Rees, B. & Mitschler, A. (1976). *J. Am. Chem. Soc.* **98**, 7918–7924.
Sakata, M. & Sato, M. (1990). *Acta Cryst.* A**46**, 263–270.
Sakata, M. & Takata, M. (1994). *MEND*. Nagoya University, Japan.
Sakata, M., Uno, T. & Takata, M. (1993). *J. Appl. Cryst.* **26**, 159–165.
Saunders, M., Fox, A. G. & Midgley, P. A. (1999). *Acta Cryst.* A**55**, 471–479.
Schneider, J. R. (1976). *J. Appl. Cryst.* **9**, 394–402.
Schneider, J. R., Hansen, N. K. & Kretschmer, H. (1981). *Acta Cryst.* A**37**, 711–722.
Smart, D. J. & Humphreys, C. J. (1980). *Inst. Phys. Conf. Ser.* No. 52, pp. 211–214.
Spence, J. C. H. & Zuo, J. M. (1992). *Electron Microdiffraction.* New York: Plenum Press.
Su, Z. & Coppens, P. (1997). *Acta Cryst.* A**53**, 749–762.
Svensson, E. C., Brockhouse, B. N. & Rowe, J. M. (1969). *Phys. Rev.* **155**, 619–632.
Tabbernor, M. A., Fox, A. F. & Fisher, R. M. (1990). *Acta Cryst.* A**46**, 165–170.
Takama, T. & Sato, S. (1982). *Philos. Mag.* B**44**, 615–626.
Temkin, R. J., Henrich, V. E. & Raccah, P. M. (1972). *Phys. Rev. B*, **6**, 3572–3581.
Zuo, J. M. (2004). *Rep Prog. Phys.* **67**, 2053–2103.